Ternary PtRuNi nanocatalysts supported on N-doped carbon nanotubes: deposition process, materials characterization, and electrochemistry

Sun, C-L.; Hsu, Y-K.; Lin, Y-G.; Chen, K-H.; Bock, C.; MacDougall, Barry; Wuy, X.; Chen, L-C.

Publisher's version / Version de l'éditeur:
https://doi.org/10.1149/1.3194800
Journal of the Electrochemical Society, 156, 10, 2009

Journal of The Electrochemical Society, **156** (10) B1249-B1252 (2009)
0013-4651/2009/156(10)/B1249/4/$25.00 © The Electrochemical Society

Ternary PtRuNi Nanocatalysts Supported on N-Doped Carbon Nanotubes: Deposition Process, Material Characterization, and Electrochemistry

Chia-Liang Sun,[a,z] Yu-Kuei Hsu,[b] Yan-Gu Lin,[b] Kuei-Hsien Chen,[b,*] Christina Bock,[c,*] Barry MacDougall,[c,] Xiaohua Wu,[d] and Li-Chyong Chen[e,*]**

[a]*Department of Chemical and Materials Engineering, Chang Gung University, Tao-Yuan 333, Taiwan*
[b]*Institute of Atomic and Molecular Sciences, Academia Sinica, Taipei 10617, Taiwan*
[c]*Institute of Chemical Process and Environmental Technologies and* [d]*Institute of Microstructural Sciences, National Research Council of Canada, Ontario K1A 0R6, Canada*
[e]*Center for Condensed Matter Sciences, National Taiwan University, Taipei 10617, Taiwan*

One-dimensional electrodes consisting of N-doped carbon nanotubes and ternary PtRuNi metal catalysts deposited via a vacuum deposition are made. Material analysis shows that high density nanoparticles that are well dispersed on the nanotube surface are deposited. The average catalyst particle size is between 3 and 4.5 nm depending on the sputtering conditions. The methanol oxidation current of the ternary PtRuNi catalysts increases up to a factor of 2.6 as compared to the binary PtRu catalyst. Our studies shed light on the advanced control of nanotube-supported electrocatalysts under a low loading via the vacuum deposition techniques and can contribute to the controlled synthesis and understanding of fuel-cell catalysts.
 [DOI: 10.1149/1.3194800]

Manuscript submitted October 7, 2008; revised manuscript received July 7, 2009. Published August 13, 2009.

Studies of electrocatalysis for fuel-cell reactions are central to the development of fuel cells (FCs).[1] More specifically, seeking the best electrode materials consisting of carbon-supported electrocatalysts plays a key role in the route toward enhanced and optimized FC performance. One-dimensional (1D) carbon nanomaterials, such as carbon nanotubes (CNTs) and nanofibers, have drawn substantial attention as the support materials for electrocatalytic nanoparticles.[2-9] It is further reported that the direct growth of CNTs on the gas diffusion layer (GDL), usually carbon cloth (CC) or carbon paper inserted between the bipolar plate and catalyst layer, can increase the output power under a low catalyst loading in FC tests.[10-12] Recently, nitrogen-doped carbon nanotubes (NCNTs) have been used in the electrode layers in FCs and supercapacitors. Regarding the catalyst support for the FC applications, Lin et al. reported that adding appropriate N doping in CNTs can prevent Pt agglomerates on pure, undoped CNTs and results in nearly monodisperse Pt nanoparticles.[13] Fang demonstrated that NCNTs can help RuO_2 and V_2O_5 dispersion and can thus obtain a higher capacitance than that obtained using undoped CNTs in supercapacitor applications.[14-16] Therefore, in this paper, we continue to put our efforts toward taking advantage of NCNTs/GDLs as the support materials for catalysts in FCs.

Pt- and PtRu-based nanoparticles with large surface-to-volume ratios have been of major interest for FCs since the 1960s.[17-19] To date, their controlled synthesis has been widely studied with respect to composition, size, shape, and facet control.[20-24] However, to the best of our knowledge, there is still limited research on the controllable synthesis of electrocatalysts on NCNTs/GDLs. Among the reported catalyst preparation methods, thin-film deposition has been employed to make a nanostructured catalyst layer.[25-29] Hence, in this work, a scalable vacuum-sputtering process is investigated to form the nanometer-sized electrocatalysts on NCNTs/GDLs.[12,30,31] Stamenkovic et al. reported that Ni can tailor the electronic structure of Pt in $Pt_3Ni(111)$ for improved oxygen reduction activity.[32] The addition of Ni to the Pt and PtRu catalysts as a possible enhancing agent for the methanol electro-oxidation reaction is also examined.[33-35] Park et al. claimed that the enhancement in the rates of methanol oxidation in their study was due to the changed electronic structure of the Pt component in PtNi and PtRuNi alloys vs those in Pt and PtRu.[33] Therefore, in this study, we use the sputtering method to fabricate binary PtRu and ternary PtRuNi nanostructured catalysts on NCNTs/CC and investigate them. The interplays between the structure and electrochemical activities of the formed catalysts on the NCNTs are addressed.

Experimental

Growth of NCNTs.— NCNTs were directly grown on CC (designation A, E-TEK) using a combination of ion beam sputtering deposition (IBSD) and microwave-plasma-enhanced chemical vapor deposition (MPECVD) techniques.[12] They are referred to here as NCNT/CC, and they served as substrates for the electrocatalysts. The iron was sputtered on the CC as a catalyst layer by IBSD to grow NCNTs on the CC. The working pressure was maintained at 5×10^{-4} Torr in an atmosphere of argon during deposition, and a Kaufman ion source was operated at a beam voltage of 1250 V and a current of 20 mA. The deposition time of the iron catalyst layer was 10 min. Following deposition, CC coated with an iron catalyst layer was then introduced to MPECVD. The hydrogen plasma treatment was operated at 1 kW and a chamber pressure of 28 Torr for 10 min. In this step, the iron catalyst layer was transformed into nanoparticles. Hydrogen plasma treatment not only reduced the iron oxides on the surface of the iron catalyst layer to the iron metal state but also generated more active catalyst sites. The NCNTs were grown in a gas mixture of $H_2/CH_4/N_2$ (80:20:80) at a microwave power of 2 kW, a chamber pressure of 45 Torr, and a substrate temperature of 900°C for 10 min.

Electrocatalyst deposition.— The physical vapor deposition (PVD) method was used to deposit platinum (Pt), ruthenium (Ru), and nickel (Ni) on the NCNT/CC substrates. Three sputtering guns (AJA International, Inc.) equipped with shutters were adopted in our multiple-gun sputtering system. When performing the sputtering process, we used a dc-reactive power generator (ENI RPG 50, MKS Instrument, Inc.) for Pt and radio-frequency (rf) power supplies and match networks (ATX-600 and RFX-600, Advanced Energy) for Ru and Ni. The sputter power for Pt and Ru was maintained at 60 and 40 W, respectively, while those for Ni were varied from 0 to 20 W. The Pt, Ru, and Ni targets were placed inside the rf planar magnetron sputtering guns in a multiple-gun PVD system. The deposition procedure was conducted for 60 min in an argon atmosphere at a working pressure of 5×10^{-2} Torr and at room temperature. The holder rotated at a constant speed (20 rpm) during deposition to yield a highly uniform coating of nanoclusters on NCNTs. There are some limitations for preparing electrocatalysts via vacuum deposi-

* Electrochemical Society Active Member.
** Electrochemical Society Fellow.
z E-mail: sunchialiang@gmail.com

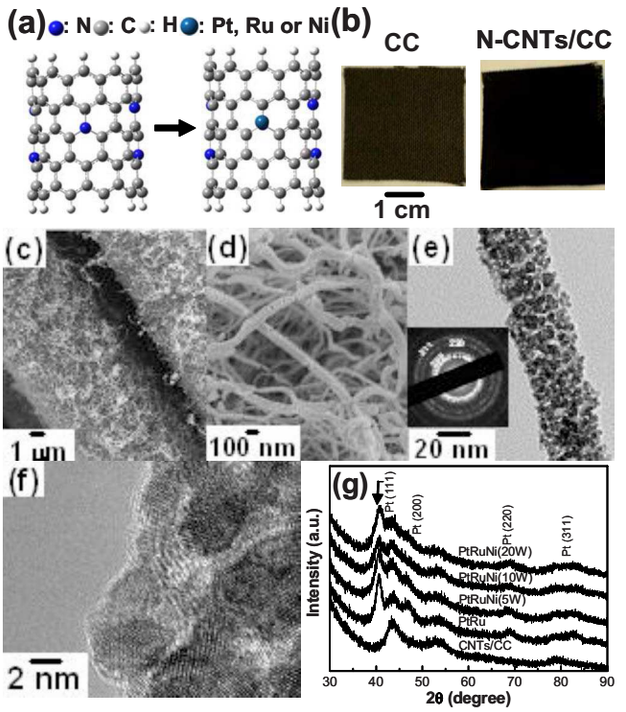

Figure 1. (Color online) (a) Atomistic models of the NCNT and metal-attached NCNT clusters. (b) E-TEK CC before and after growing NCNTs. (c) SEM images of NCNTs on CC. (d) High magnification SEM images of electrocatalyst-coated NCNTs. (e) TEM image of a single nanocable. Inset is the corresponding selected area electron diffraction pattern of Pt-based alloy. (f) High resolution TEM image of nanosized catalysts on nanocable surface. (g) XRD patterns of nanocable electrodes fabricated under a variety of sputtering conditions.

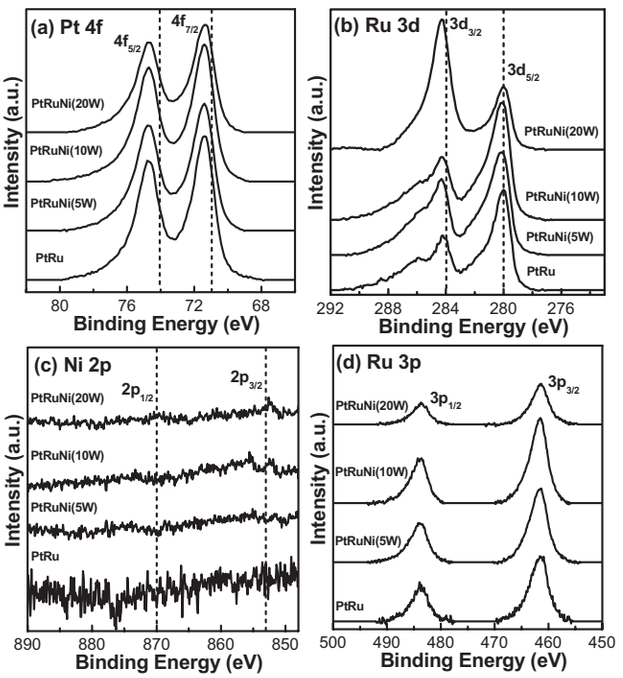

Figure 2. XPS (a) Pt 4f, (b) Ru 3d, (c) Ni 2p, and (d) Ru 3p spectra of 1D composite nanoelectrodes synthesized at different Ni sputtering powers.

tion. For example, the carbon support should be kept dry due to the requirement of vacuum in the processing. Through vacuum deposition, the catalyst layer with uniform distribution is relatively thin because of the shadow effect compared with the conventional method.

Electrochemical testing of the NCNT/CC-supported catalysts.— Electrocatalyst-coated NCNT/CC substrates were formed into working electrodes by attaching a Au wire. Both sides of the working electrodes were exposed to the electrolyte solution. Three compartment cells, in which the reference electrode was separated from the working and counter electrode compartments by a Luggin capillary, were employed for the electrochemical studies. A saturated calomel electrode (SCE) was used as the reference electrode. However, all potentials in this work are reported vs the reversible hydrogen electrode (RHE) using a potential difference for SCE vs RHE. A large surface area Pt gauze served as the counter electrode. American Chemical Society grade chemicals and high resistivity 18 MΩ water were used. CO was adsorbed onto the electrodes at 0.15 V by bubbling CO gas through the 0.5 M H_2SO_4 solution for 20 min. CO solution was subsequently removed by bubbling high purity argon gas for 40 min, maintaining the potential at 0.15 V. The potential was then cycled for two cycles at a rate of 10 mV s^{-1}. The intersection between the CO_{ads} oxidation peak and its background in the first two cycles was picked up as onset potential (E_{on}).

Instrumentations and techniques.— Electrochemical experiments were performed using a Solartron SI 1287 potentiostat/galvanostat (Solartron Group Ltd.) computer controlled by Corrware software (Scribner Assoc.). A Bruker D8 advance X-ray diffraction (XRD) system was employed to obtain XRD patterns. The scanning angle 2θ extended from 30 to 90°. X-ray photoelectron spectroscopy (XPS) spectra were obtained using a Kratos Axis Ultra spectrometer. A Hitachi S-4800 scanning electron microscope (SEM) and a transmission electron microscope (TEM, JEOL JEM-2100F) were employed to obtain morphological information on the catalyst samples

Table I. Characteristics of 1D composite nanoelectrodes.

Catalyst[a] (W)	Pt[b] (atom %)	Ru[b] (atom %)	Ni[b] (atom %)	d_{220}[c] (nm)	I_{peak}[d] (mA/cm^2)	E_{on}[e] (V)	E_{fwhm}[e] (mV)
PtRu	49.1	50.9	0	4.5	5.6	0.44	147 ± 18
PtRuNi (5 W)	44.8	53.3	1.9	3.8	9.2	0.45	165 ± 18
PtRuNi (10 W)	43.5	53.0	3.5	3.0	14.5	0.46	159 ± 13
PtRuNi (20 W)	49.6	45.8	4.6	3.5	11.6	0.40	85 ± 9

[a] The numbers in brackets denote the Ni gun powers in multiple-gun magnetron sputtering process.
[b] Pt:Ru:Ni surface ratios were derived from the XPS spectra.
[c] The average particle sizes were determined by resolving the Scherrer equation using Pt-based (220) peaks in Fig. 1g.
[d] Methanol oxidation currents were recorded in forward scans in Fig. 3a.
[e] E_{on} and E_{fwhm} ($CO_{ads} \rightarrow CO_2$) were estimated using CO_{ads} oxidation peaks in Fig. 3b. These potentials are referred to the RHE.

and substrates. The mass per unit area of the metals was determined by inductively coupled plasma–optical emission spectroscopy (ICP-OES, PerkinElmer ICP-OES Optima 125 3000). In this paper, all samples were loaded with approximately 0.2 mg Pt per geometry area of each square centimeter.

Results and Discussion

Figure 1a shows the atomistic models of N dopants in zigzag (10,0) nanotube clusters with and without metal attachment.[31,32] It is reported that the extrinsic N dopants can help metal catalyst dispersion on NCNTs.[12-16,30,31] Therefore, we suggest that the metal atom stays around the N dopant sites in our models. Figure 1b-d illustrates the morphology of NCNTs directly grown on the E-TEK CC. In Fig. 1b, the E-TEK CC with the NCNTs on top turns black compared with the "as-received" gray CC sample on the left side. Figure 1c shows that the porous CC is the ensemble of carbon fibers with diameters of several tens of micrometers as a GDL. Figure 1c, shows that a thin NCNT layer can be directly grown on the surface of carbon fibers. Subsequently, the magnetron sputtering is performed to deposit Pt, Ru, and Ni on NCNTs/CC. After sputtering, the high magnification SEM image in Fig. 1d shows the high surface area, catalyst-coated NCNT. Figure 1e is the TEM micrograph of a single catalyst-coated NCNT with a darker contrast than the uncoated CNT. It is quite clear that PVD can generate high density nanocatalysts on the sidewall to form the shell of a nanocable. In Fig. 1f, the clear lattice fringe of the nanocrystals, with the particle size as small as several nanometers, is observed. Figure 1g shows the XRD patterns of multicomponent catalysts deposited on NCNT/CC. Notice that the full width at half-maximum (fwhm) of the Pt peak changes along with the adjustment of the Ni sputtering power when the power for Pt and Ru is kept constant. Comparing all the (220) peaks, the minimal particle size of 3.0 nm is derived for PtRuNi (10 W). This size change is attributed to the modified nucleation and growth of nanocatalysts on NCNTs, resulting in different particle sizes and densities after adding Ni to the sputtering process. The shift of XRD peaks of PtRuNi, relative to those in PtRu, is ascribed to the change in their lattice spacing with Ni.

Figure 2 displays XPS Pt 4f, Ru 3d, Ni 2p, and Ru 3p spectra of 1D composite nanoelectrodes synthesized at different Ni sputtering powers. The dashed lines indicate the peak position for each zero-valence transition metal. Positive shifts of Pt $4f_{5/2}$ and Pt $4f_{7/2}$ from those of pure Pt were observed on all alloy samples, suggesting the lowering of the Fermi level or the increase in the valence electron vacancy.[36,37] These shifts suggest that Ru and Ni alter the electronic structure of Pt and could enhance the catalytic activity of Pt for methanol oxidation. In all alloys, the shoulder of Ru $3d_{3/2}$ and Ru $3d_{5/3}$ in high binding energy corresponds to the existence of RuO_2 and RuO_3; these oxidation states aid in improving methanol oxidation by providing Pt-bonded CO with oxygen species.[33,34] The profound Ru $3d_{3/2}$ peak in PtRuNi (20 W) catalyst reveals the changed electronic structure of Ru with a sufficient amount of Ni and could improve its ability to remove CO on Pt. The less intense Ru 3p region was also analyzed in addition to the main Ru 3d spectra, as the latter overlays the C 1s region. At Ni-containing catalysts, the Ni additive comprises metallic Ni, NiO, $Ni(OH)_2$, and NiOOH.[33] The Ni contents in composite electrodes increase from 0 to 4.6 atom % along with the increasing Ni sputtering power, as indicated in Table I.

Besides the above-mentioned material analysis results, we further carried out electrochemical measurements relevant to methanol oxidation. Figure 3a illustrates cyclic voltammograms (CVs) of the composite electrodes in 1 M CH_3OH + 1 M H_2SO_4 solutions at a scan rate of 50 mV s^{-1}. The current scale is normalized using the geometrical electrode area. Clearly, the PtRuNi catalysts always have considerably higher peak currents than the binary PtRu. The high I_{peak} of the PtRuNi (10 W) catalyst is attributed to the large reaction surface area associated with the small particle size, as revealed by XRD. When the power of the sputtering gun changes, the electrochemical surface areas of the catalysts also change. Accord-

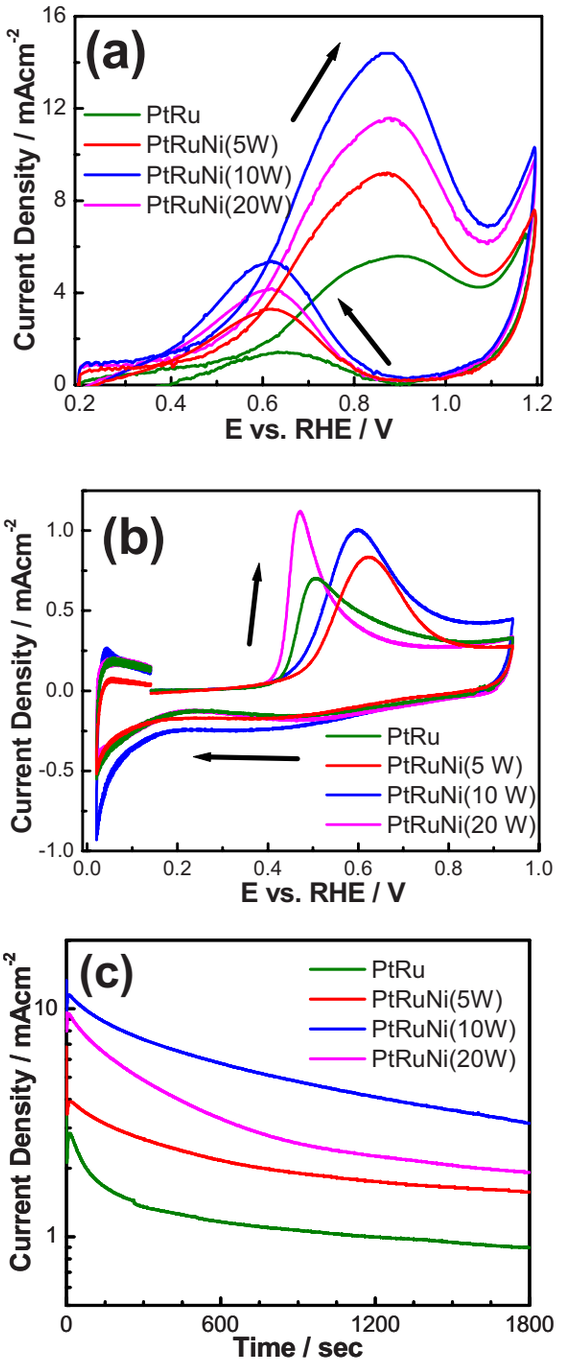

Figure 3. (Color online) (a) CVs recorded at 50 mV s^{-1} in 1 M CH_3OH + 1 M H_2SO_4 solutions for composite nanoelectrodes with different Ni contents. (b) CO_{ads} stripping voltammograms (the first cycle) recorded at 10 mV s^{-1} in 0.5 M H_2SO_4 solution. (c) Chronoamperometric measurements of nanocable electrodes fabricated under a variety of sputtering conditions recorded at the potential of 0.65 V in 1 M CH_3OH + 1 M H_2SO_4 solutions.

ing to the calculations in the hydrogen adsorption region, the PtRuNi (10 W) catalyst has the highest electrochemical surface area, which is consistent with the XRD result. When the particle size of the catalysts becomes smaller, their electrochemical surface area gets higher. CO-adsorbed (CO_{ads}) stripping voltammograms were further employed to investigate nanoparticle surfaces in solution en-

vironments. In Fig. 3b, the increase in the CO_{ads} stripping peak area of PtRuNi catalysts has a trend similar to that shown in I_{peak}, as a consequence of an altered particle size. More importantly, the onset potentials (E_{on}) for the CO_{ads} oxidation reactions for all catalysts occur between 0.40 and 0.46 V vs RHE and are comparable to those of PtRu.[38,39] This benefit is assigned to the bifunctional mechanism, i.e., the formation of "Ru–OH" species to release CO-poisoned Pt sites on particle surfaces starting at low potentials.[18] The CO_{ads} oxidation reaction is thought to take place according to the bifunctional mechanism as follows

$$Ru + H_2O \rightarrow Ru\text{–}OH + H^+ + e^- \quad [1]$$

$$M\text{–}CO + Ru\text{–}OH \rightarrow M + Ru + CO_2 + H^+ + e^- \quad [2]$$

In Eq. 2, M can be a single Pt, Ru, or Ni monoatomic site on the catalyst surface onto which CO can absorb. As indicated in Fig. 3b, the lowest E_{on} and the narrowest potential fwhm (E_{fwhm}) are observed for the PtRuNi (20 W) catalyst, suggesting a better oxidation kinetics for the complete CO_{ads} to CO_2 oxidation than other catalysts. This advantage in CO_{ads} oxidation kinetics is likely due to the modified atomistic distribution, electronic structure, and particle size of the catalyst particles and their individual components.[40,41] In Fig. 3c, the chronoamperometric measurements show that the PtRuNi (10 W) catalyst has the highest performance for methanol oxidation.

Conclusion

The preparation and performance of NCNT-supported PtRuNi electrocatalysts are reported. Compared to the PtRu catalyst, the PtRuNi catalyst exhibits a higher methanol oxidation current and a lower CO_{ads} stripping potential. Our studies shed light on the advanced control of nanometer-sized catalysts on 1D NCNTs for FC technologies.

Acknowledgments

The authors gratefully acknowledge the financial support from the National Science Council of Taiwan, the National Research Council of Canada, and AFOSR/AOARD. We thank D. Kingston (NRC, Ottawa) for his assistance with SEM and XPS.

Chang Gung University assisted in meeting the publication costs of this article.

References

1. S. Srinivasan, *Fuel Cells: From Fundamentals to Applications*, Springer, New York (2006).
2. G. Che, B. B. Lakshmi, E. R. Fisher, and C. R. Martin, *Nature (London)*, **393**, 346 (1998).
3. C. A. Bessel, K. Laubernds, N. M. Rodriguez, and R. T. K. Baker, *J. Phys. Chem. B*, **105**, 1115 (2001).
4. Z. L. Liu, X. H. Lin, J. Y. Lee, W. Zhang, M. Han, and L. M. Gan, *Langmuir*, **18**, 4054 (2002).
5. E. S. Steigerwalt, G. A. Deluga, and C. M. Lukehart, *J. Phys. Chem. B*, **106**, 760 (2002).
6. W. Z. Li, C. H. Liang, W. J. Zhou, J. S. Qiu, Z. H. Zhou, G. Q. Sun, and Q. Xin, *J. Phys. Chem. B*, **107**, 6292 (2003).
7. G. Girishkumar, K. Vinodgopal, and P. V. Kamat, *J. Phys. Chem. B*, **108**, 19960 (2004).
8. C. Kim, Y. J. Kim, T. Yanagisawa, K. C. Park, M. Endo, and M. S. Dresselhaus, *J. Appl. Phys.*, **96**, 5903 (2004).
9. S. Liao, K. A. Holmes, H. Tsaprailis, and V. I. Briss, *J. Am. Chem. Soc.*, **128**, 3504 (2006).
10. X. Sun, R. Li, D. Viller, J. P. Dodelet, and S. Desilets, *Chem. Phys. Lett.*, **379**, 99 (2003).
11. C. Wang, M. Waje, X. Wang, J. M. Tang, R. C. Haddon, and Y. Yan, *Nano Lett.*, **4**, 345 (2004).
12. C. H. Wang, H. Y. Du, Y. T. Tsai, C. P. Chen, C. J. Huang, L. C. Chen, K. H. Chen, and H. C. Shih, *J. Power Sources*, **171**, 55 (2007).
13. Y. G. Lin, Y. K. Hsu, C. T. Wu, S. Y. Chen, K. H. Chen, and L. C. Chen, *Diamond Relat. Mater.*, **18**, 433 (2009).
14. W. C. Fang, *Nanotechnology*, **19**, 165705 (2008).
15. W. C. Fang and W. L. Fang, *Chem. Commun. (Cambridge)*, **2008**, 5236.
16. W. C. Fang, K. H. Chen, and L. C. Chen, *Nanotechnology*, **18**, 485716 (2007).
17. J. O'M. Bockris and H. Wroblowa, *J. Electroanal. Chem.*, **7**, 428 (1964).
18. M. Watanabe and S. Motoo, *J. Electroanal. Chem. Interfacial Electrochem.*, **60**, 267 (1975).
19. M. Watanabe, in *Catalysis and Electrocatalysis at Nanoparticle Surfaces*, A. Wieckowski, E. R. Savinova, and C. G. Vayenas, Editors, pp. 827–845, Marcel Dekker, New York (2003).
20. E. Reddington, A. Sapienza, B. Gurau, R. Viswanathan, S. Sarangapani, E. S. Smotkin, and T. E. Mallouk, *Science*, **280**, 1735 (1998).
21. C. Bock, C. Paquet, M. Couillard, E. A. Botton, and B. R. MacDougall, *J. Am. Chem. Soc.*, **126**, 8028 (2004).
22. C. Burda, X. Chen, R. Narayanan, and M. A. El-Sayed, *Chem. Rev. (Washington, D.C.)*, **105**, 1025 (2005).
23. T. He, E. Kreidler, L. Xiong, J. Luo, and C. J. Zhong, *J. Electrochem. Soc.*, **153**, A1637 (2006).
24. N. Tian, Z.-Y. Zhou, S.-G. Sun, Y. Ding, and Z. L. Wang, *Science*, **316**, 732 (2007).
25. M. K. Debe, in *Handbook of Fuel Cells, Fundamentals, Technology and Applications*, Vol. 3, W. Vielstich, A. Lamm, and H. A. Gasteiger, Editors, pp. 576–589, John Wiley & Sons, Chichester, U.K. (2003).
26. C. K. Witham, W. Chun, T. I. Valdez, and S. R. Narayanan, *Electrochem. Solid-State Lett.*, **3**, 497 (2000).
27. A. T. Haug, R. E. White, J. W. Weidner, W. Huang, S. Shi, N. Rana, S. Grunow, T. C. Stoner, and A. E. Kaloyeros, *J. Electrochem. Soc.*, **149**, A868 (2002).
28. T. Nakakubo, M. Shibata, and K. Yasuda, *J. Electrochem. Soc.*, **152**, A2316 (2005).
29. P. Bommersbach, M. Mohamedi, and D. Guay, *J. Electrochem. Soc.*, **154**, B876 (2007).
30. C. L. Sun, L. C. Chen, M. C. Su, L. S. Hong, O. Chyan, C. Y. Hsu, K. H. Chen, T. F. Chang, and L. Chang, *Chem. Mater.*, **17**, 3749 (2005).
31. C. L. Sun, H. W. Wang, M. Hayashi, L. C. Chen, and K. H. Chen, *J. Am. Chem. Soc.*, **128**, 8368 (2006).
32. V. R. Stamenkovic, B. Fowler, B. S. Mun, G. Wang, P. N. Ross, C. A. Lucas, and N. M. Marković, *Science*, **315**, 493 (2007).
33. K. W. Park, J. H. Choi, B. K. Kwon, S. A. Lee, Y. E. Sung, H. Y. Ha, S. A. Hong, H. Kim, and A. Wieckowski, *J. Phys. Chem. B*, **106**, 1869 (2002).
34. J. H. Choi, K. W. Park, B. K. Kwon, and Y. E. Sung, *J. Electrochem. Soc.*, **150**, A973 (2003).
35. A. Gore, U.S. Pat. 6,921,605 (2005).
36. T. Toda, H. Igarashi, and M. Watanabe, *J. Electrochem. Soc.*, **145**, 4185 (1998).
37. T. Toda, H. Igarashi, H. Uchida, and M. Watanabe, *J. Electrochem. Soc.*, **146**, 3750 (1999).
38. C. Bock, B. MacDougall, and Y. LePage, *J. Electrochem. Soc.*, **151**, A1269 (2004).
39. C. Bock, M.-A. Blakely, and B. MacDougall, *Electrochim. Acta*, **50**, 2401 (2005).
40. B.-J. Hwang, L. S. Sarma, J.-M. Chen, C.-H. Chen, S.-C. Shih, G.-R. Wang, D.-G. Liu, J.-F. Lee, and M.-T. Tang, *J. Am. Chem. Soc.*, **127**, 11140 (2005).
41. D.-Y. Wang, C.-H. Chen, H.-J. Yan, Y.-L. Lin, P.-Y. Huang, B.-J. Hwang, and C.-C. Chen, *J. Am. Chem. Soc.*, **129**, 1538 (2007).